Synthesis of Heteroaryl Imines: Theoretical and Experimental Approach to the Determination of the Configuration of CN Double Bond

ARTICLE *in* THE JOURNAL OF ORGANIC CHEMISTRY · OCTOBER 2006

Impact Factor: 4.72 · DOI: 10.1021/jo0605501 · Source: PubMed

6 AUTHORS, INCLUDING:

Maurizio D'Auria
Università degli Studi della Basilicata
366 PUBLICATIONS **2,765** CITATIONS
SEE PROFILE

Maria Funicello
Università degli Studi della Basilicata
65 PUBLICATIONS **568** CITATIONS
SEE PROFILE

Francesco Lelj
Università degli Studi della Basilicata
218 PUBLICATIONS **3,566** CITATIONS
SEE PROFILE

Rocco Racioppi
Università degli Studi della Basilicata
115 PUBLICATIONS **724** CITATIONS
SEE PROFILE

JOC*Article*

Synthesis of Heteroaryl Imines: Theoretical and Experimental Approach to the Determination of the Configuration of C=N Double Bond

Mario Amati,[†] Carlo Bonini,*[,‡] Maurizio D'Auria,*[,‡] Maria Funicello,[‡] Francesco Lelj,*[,†] and Rocco Racioppi[‡]

Dipartimento di Chimica, Università della Basilicata, Via N. Sauro 85, 85100 Potenza, Italy, and LAMI Dipartimento di Chimica, LASCAMM-INSTM, Università della Basilicata, Via N. Sauro 85, 85100 Potenza, Italy

dauria@unibas.it

Received March 13, 2006

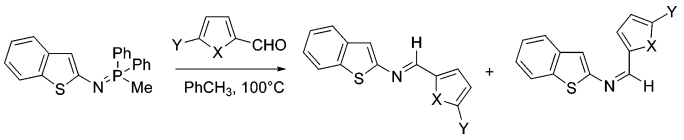

The reaction between an iminophosphorane with furan-2-carbaldehyde, thiophene-2-carbaldehyde, furan-3-carbaldehyde, and thiophene-3-carbaldehyde at 60 °C gives the corresponding *trans* imines in 53−84% yields, while the same reaction at 100 °C gives a mixture of the corresponding *trans* and *cis* imines. Whether the iminophosphorane reacted with 5-nitrofuran-2-carbaldehyde or 5-nitrothiophene-2-carbaldehyde only the *trans* imines were obtained in 85−89% yields. The irradiation of the imines obtained from thiophene-2-carbaldehyde and thiophene-3-carbaldehyde gave the corresponding photocyclization products. *Cis*/*trans* stereochemistry of the imines can be assigned simulating the UV−vis spectra. In the case of the imine from furan-2-carbaldehyde the computed spectra are characterized by an intense absorption at 361 and 357 nm respectively for the *trans*-1 and *trans*-2 structures. No other absorptions of comparable intensity have been predicted: the agreement with the experimental spectrum can be considered good. Furthermore, the experimental weak peaks at 280 and 270 nm can be associated to the computed transitions at 278 and 260 nm for the *trans*-1 isomer. Several minima of the energy surface can be assigned to the *cis* isomer, and they all present a very similar energy. The structures of the *cis*-1 and *cis*-2 isomers present quite coincident computed electronic spectra. In both cases, the computed spectrum shows two principal features. For the *cis*-1 structure, the first characteristic absorption is located at 414 nm and the second one at 284 nm. For the *cis*-2 structure, the first feature is located at 412 nm and the second one at 286 nm. The second transition is computed somewhat more intense. The experimental spectrum could be the consequence of similar populations of the planar *cis* structure (*cis*-3) and nonplanar *cis* structures (*cis*-1, *cis*-2, and their enantiomers).

Introduction

In recent years the iminophosphoranes have been revealed to be useful intermediates for the synthesis of nitrogen-containing heterocycles. Such compounds, first synthesized in 1919 by Staudinger from azides and triphenylphosphine, became useful intermediates because of their application in the aza-Wittig reaction to give imines that, often without isolation, can electrocyclize to pyridine or pyrimidine rings.[1]

In our research studies on benzothiophene chemistry we have recently synthesized either 2- or 3-benzothienyl iminophosphoranes starting from the corresponding heteroaryl azides together with aryl- and/or alkyl-substituted phosphines. *N*-(3-Benzothienyl)iminotriphenylphosphorane has been used in the aza-Wittig reaction with α,β-unsaturated aldehydes in mild reaction conditions to afford pyridines *b*-fused on benzothiophene without isolation or other evidence of iminic product as intermediate (Scheme 1).[2]

[†] LAMI-LASCAMM-INSTM, Potenza.
[‡] Department of Chemistry, Potenza.

(1) (a) Barluenga, J.; Palacios, F. *Org. Prep. Proced. Int.* **1991**, 1. (b) Gologlogov, Y. G.; Kausukhin, L. F. *Tetrahedron* **1992**, *48*, 1353−1406. (c) Molina, P.; Vilaplana, M. J. *Synthesis* **1994**, 1197−1218. (d) Wamhoff, H.; Richardt, G.; Stolben, S. *Adv. Heterocycl. Chem.* **1995**, *64*, 159−249. (e) Funicello, M.; Spagnolo, P. In *Targets in Heterocyclic Chemistry*; Attanasi, O. A., Spinelli, D., Eds.; Italian Society of Chemistry: Rome, Italy, 2004; Vol. 8, pp 274−287.

10.1021/jo0605501 CCC: $33.50
Published on Web 08/16/2006

SCHEME 1. The Reaction between 3-Benzothienyl Iminophosphorane and α,β-Unsaturated Aldehydes

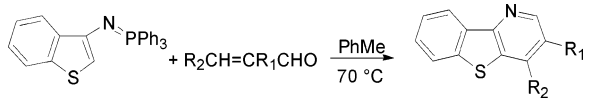

SCHEME 2. The Reaction of 3-Benzothienyl Iminophosphoranes and α,β-Unsaturated Carbonyl Compounds

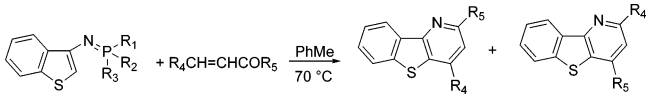

SCHEME 3. Synthesis of 2-Benzothienyl Iminophosphorane and Reactivity toward α,β-Unsaturated Aldehydes

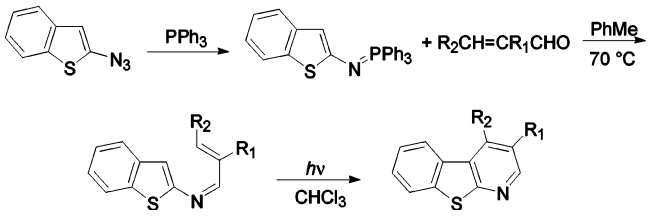

N-(3-Benzothienyl)iminodiphenylmethyl- and dimethylphenylphosphoranes have also been synthesized and tested in the aza-Wittig reaction with α,β-unsaturated aldehydes and ketones: surprisingly in such reactions, two isomeric benzothienopyridines have been isolated in different ratios depending on the composition of the used phosphoranes or on the α,β-unsaturated compound (Scheme 2).[3]

On the basis of *N*-(3-benzothienyl)iminophosphorane behavior we hypothesized that also *N*-(2-benzothienyl)iminophosphorane could behave in the same way; therefore, we decided to test it in the aza-Wittig reaction with α,β-unsaturated compounds already used for the 3-isomer. In this case, the aza-Wittig reaction afforded first the iminic product (often isolated and characterized) that cyclized only after UV irradiation in chloroform solution. When the reaction was performed with aromatic and heteroaromatic aldehydes we could isolate only the corresponding imine, and sometimes two imines that were revealed to be very stable compounds (Scheme 3).[4]

In this paper we describe the synthesis, characterization, and photoreactivity of a series of new heteroarylimines. However, in this study we found difficulty in assigning *cis*−*trans* stereochemistry of the prepared imines; we wish to present a solution to this problem based on the analysis of UV−vis spectra. We will finally assign the *cis*−*trans* stereochemistry of the iminic product by discussing the obtained results reporting an exhaustive theoretical approach with calculation and prevision of the UV−vis spectra of the *cis* and *trans* imines and their experimental UV−vis confirmation.

Result and Discussion

Preparation and Photoreactivity of Heteroarylimines. The most common method for the synthesis of imines is represented by the condensation of a carbonilic compound and an aminic precursor. Since in heterocyclic chemistry amines often show low stability, which prevents this simple route (leading to low yields and several byproducts), we have instead used an aza-Wittig reaction of iminophosphoranes with 2- and 3-thiophencarboxaldehyde and 2- and 3-furancarboxaldehyde.

SCHEME 4. The Reaction of the Iminophosphorane 1 with Heteroaromatic Aldehydes

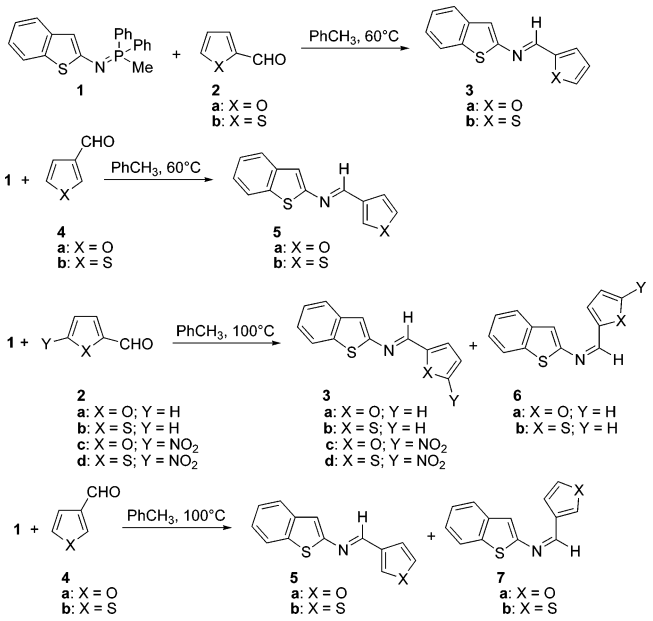

TABLE 1. The Reaction between the Iminophosphorane 1 and Heteroaromatic Aldehydes

entry	aldehyde	temp [°C]	imine	yield [%]
1	furan-2-carbaldehyde	60	**3a**	53
2	thiophene-2-carbaldehyde	60	**3b**	84
3	furan-3-carbaldehyde	60	**5a**	54
4	thiophene-3-carbaldehyde	60	**5b**	53
5	furan-2-carbaldehyde	100	**3a**	50
			6a	30
6	thiophene-2-carbaldehyde	100	**3b**	67
			6b	33
7	furan-3-carbaldehyde	100	**5a**	44
			7a	28
8	thiophene-3-carbaldehyde	100	**5b**	42
			7b	21
9	5-nitrofuran-2-carbaldehyde	100	**3c**	85
10	5-nitrothiophene-2-carbaldehyde	100	**3d**	89

We performed the reaction at 60 °C in toluene with an equimolar ratio of the opportune aldehydic precursors and of the iminophosphorane **1**, which in previous experiments was shown to be the reagent of choice.[3,4] In such conditions only a single product was obtained (Scheme 4, Table 1); when the reaction was carried out at 100 °C two products were obtained (Scheme 4, Table 1). After purification of the crude reaction we characterized the two main products assigning them the iminic structure on the basis of the diagnostic ^{1}H resonance value of CH═N at about 8.4 ppm. Obviously, the correct *cis*−*trans* structure of the imine could be assigned only after the theoretical approach described below: however, for the reader's convenience, we anticipate the structures of the obtained products in Scheme 4 and Table 1.

The reaction between the iminophosphorane **1** with furan-2-carbaldehyde at 60 °C afforded the *trans* imine **3a** in 53% yield, while the same reaction at 100 °C gave a mixture of the *trans*

(2) Degl'Innocenti, A.; Funicello, M.; Scafato, P.; Spagnolo, P.; Zanirato, P. *J. Chem. Soc., Perkin Trans. 1* **1996**, 2561−2563.
(3) Bonini, C.; Chiummiento, L.; Funicello, M.; Spagnolo, P. *Tetrahedron* **2000**, *56*, 1517−1521.
(4) Bonini, C.; D'Auria, M.; Funicello, M.; Romaniello, G. *Tetrahedron* **2002**, *58*, 3507−3512.

imine **3a** and the *cis* isomer **6a** in 50% and 30% yield, respectively. For the assignment of *trans/cis* stereochemistry see below. The same reaction on thiophene-2-carbaldehyde at 60 °C gave the *trans* imine **3b** in 84% yield, while at 100 °C the *trans* imine **3b** was obtained in 67% yield in the presence of 33% of the *cis* isomer **6b**. The reaction between the iminophosphorane **1** with furan-3-carbaldehyde gave at 60 °C the *trans* imine **5a** in 54% yield and at 100 °C a mixture of the *trans* imine **5a** and the *cis* isomer **7a** in 44% and 28% yields, respectively. When the iminophosphorane **1** reacted with thiophene-3-carbaldehyde at 60 °C the *trans* imine **5b** was obtained in 53% yield, when the same reaction was performed at 100 °C the *trans* imine **5b** was obtained in 42% yield, while the *cis* isomer **7b** was isolated with an overall yield of 21%. Whether the iminophosphorane **1** reacted with 5-nitrofuran-2-carbaldehyde and 5-nitrothiophene-2-carbaldehyde only the *trans* imines were obtained in very good yields.

The described condensation processes performed at 60 and 100 °C showed a definite trend in the amounts of two main products. In particular, the increasing temperature also favors the yield of the most abundant product. This increase appears to be independent of the particular composition (X = O, S) and on the position of the aldehydic substitution (C-2 or C-3 substituents). The presence of *trans*−*cis* isomerization is well documented,[5] suggesting that the most abundant product is the *trans* isomer. On the other hand, a direct experimental proof is necessary to give a more thorough description of the addition reactions in this class of compounds (see below).

Imines can be used as substrates for photocyclization reactions.[5d] On the contrary, this type of substrate is recalcitrant toward (2+2) cycloaddition reactions. Therefore, we have tested the photochemical reactivity of our prepared substrates (see Scheme 5): the photocyclization was attempted by exposing both *cis* and *trans* imines to the UV lamp ($\lambda \geq 300$ nm) for 6−8 h in a large variety of solvents. After exposure the *trans* imines often remained unaltered while *cis* imines were converted to new compounds **8** and **9** when the reaction was performed on the imine derived from thiophene-2- and thiophene-3-carbaldehyde (Scheme 5).[4] Unfortunately, both *trans* and *cis* imines obtained from furan-2-carbaldehyde and furan-3-carbaldehyde gave decomposition products when irradiated.

It is interesting to note that the C═N bond can give photochemical *trans*−*cis* isomerization.[6] The reaction occurs through a conical intersection between S_1 and S_0 states.[6b] We tested that **3b**, a compound unable to give *trans*−*cis* photochemical isomerization, did not show a fluorescence spectrum. This result can be in agreement with an efficient intersystem crossing to the excited triplet state, unable to give, on these compounds, a photochemical isomerization.

Determination of Cis−Trans Configuration of Imines 3a and 5a: Computations and Experimental UV−Vis Absorption Spectra. A simple and direct proof of the isomer structure was been hampered by some difficulties. Due to the lack of meaningful NOE effects, mainly for eventual conformational flexibility and the large distance between the appropriate iminic and aromatic H protons, it was impossible to use this powerful technique to unambiguously assign the geometric configuration to the isolated isomers.

Furthermore, no good-quality crystals could be grown in order to perform an X-ray diffraction characterization.

In our study the powerful UV spectroscopy was also carefully utilized but the different spectra were obtained in the case of the different kinds of products (see Figures 4 and 12 and the experimental part for detailed spectra): however, the qualitative differences we have found could not be easily assigned to the *cis* or *trans* configuration, owing also to the possible conformational flexibility of the compounds.

To circumvent these difficulties a combination of ab initio conformational analysis at DFT level and electronic excitation spectra calculated by means of the TD-DFT approach has been therefore undertaken, also based on previous similar studies for the *trans*−*cis* configuration of different oximes.[7]

SCHEME 5. Photochemical Behavior of Trans and Cis Imines

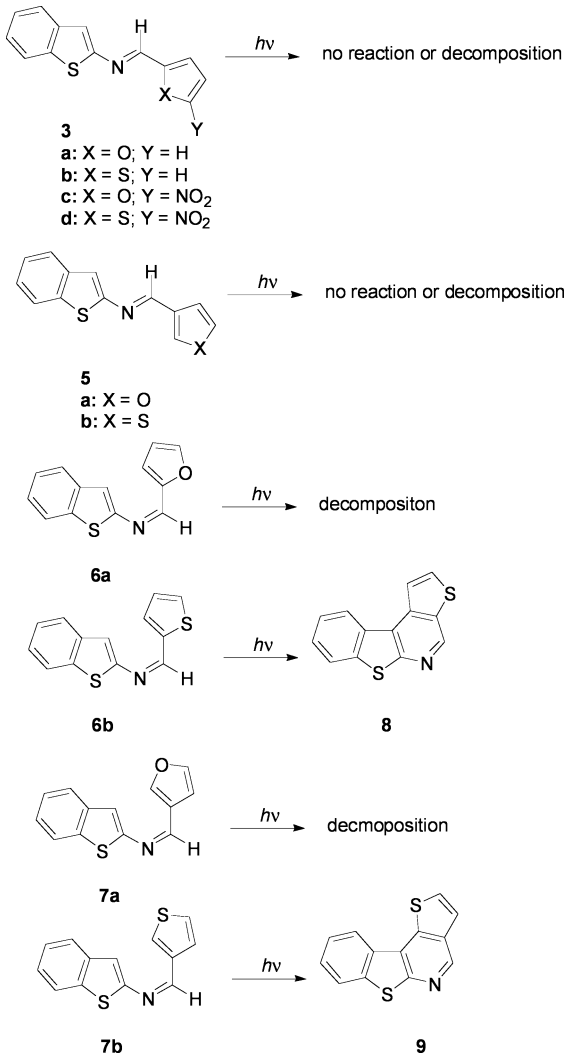

(5) For C═N thermal and/or photochemical isomerization: (a) Curtin, D. Y.; Hausser J. W. *J. Am. Chem. Soc.* **1961**, *83*, 3474−3481. (b) Raban, M.; Carlson, E. *J. Am. Chem. Soc.* **1971**, *93*, 685−691. (c) Marcoccia, J. F.; Yates, K.; Csizmadia, I. G. *J. Mol. Struct.* (*THEOCHEM*) **1996**, *360*, 1−39. (d) Padwa, A. *Chem. Rev.* **1977**, *77*, 37−68. (e) Stepanenko, T.; Lapinski, L.; Sobolewski, A. L.; Nowak, M. J.; Kierdaszuk, B. *J. Phys. Chem. A* **2000**, *104*, 9459−9466. (f) King, N. R.; Whale, E. A.; Davis, F. J.; Gilbert, A.; Mitchell, G. R. *J. Mater. Chem.* **1997**, *7*, 625−630. (g) Johnson, J. E.; Morales, N. M.; Gorczyca, A. M.; Dolliver, D. D.; McAllister M. A. *J. Org. Chem.* **2001**, *66*, 7979−7985.

(6) (a) Paetzold, R.; Reichenbächer, M.; Appenroth, K. *Z. Chem.* **1981**, *21*, 421−430. (b) Bonăcić-Koutecký, V.; Michl, J. *Theor. Chim. Acta* **1985**, *68*, 45−55.

(7) Stepanenko, T.; Lapinski, L.; Nowak, M. J.; Adamowicz, L. *Vib. Spectrosc.* **2001**, *26*, 65−82.

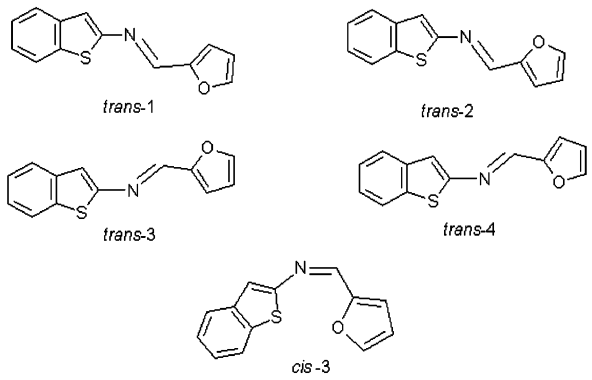

FIGURE 1. Possible conformers of the imines obtained in the reaction between furan-2-carbaldehyde and **1**.

Figure 1 collects the possible conformers of the imines obtained from furan-2-carbaldehyde assuming a planar arrangement around each bond. They have been labeled as *trans* and *cis* isomers according to the stereochemistry around the iminic function. For the *trans* isomers, all four possible isomers are shown, whereas for the *cis* isomers, only one of the four analogues isomers has been shown for reasons which will become clear below.

According to our computational work, energy minima associated with the four *trans* structures of Figure 1 can be found. *trans*-1 and *trans*-2 isomers are planar structures, whereas *trans*-3 and *trans*-4 present not-parallel average planes of the benzothiophene and furan rings. Since the iminic bridge roughly lies on the average plane of the furan ring, the dihedral angle between the two average planes can be approximated with the torsion angle 1−2−3−4 (named χ_1 afterward), which amounts to 152.1° for the *trans*-3 structure (Figure 2). The *trans*-4 structure shows a similar structure, with a torsion angle of 150.9°.

TABLE 2. Relative Energies of All the Structures of the Imines from Furan-2-carbaldehyde and 1

isomer	electronic energy (kcal/mol)	ΔG^0 (kcal/mol)
trans-1	0.0	0.0
trans-2	+0.9	+1.0
trans-3	+2.5	+2.6
trans-4	+3.6	+3.7
cis-1	+7.2	+7.4
cis-2	+7.8	+8.0
cis-3	+7.3	+7.4

Since nonplanar *trans*-3 and *trans*-4 structures are asymmetric, two enantiomeric structures (we name them *σ-trans*-3 and *σ-trans*-4) must exist. However, as pointed out below, their existence is not important for the issue raised in this paper, and they will not be further discussed.

Among all the *trans* isomers (reported in Table 2) the *trans*-1 is the lowest in energy.

With respect to the *cis* isomers, five relative minima on the energy surface have been found. As showed in Figure 2, two structures are not planar. Also in these cases, the iminic function approximately lies on the average plane of the furan ring, but this plane is rotated relative to the average plane of the benzothiophene ring. Thus, we can use the same torsion angle χ_1 (dihedral angle 1−2−3−4 in Figure 2) for measuring the dihedral angle between the two planes. For the *cis*-1 structure, χ_1 is estimated to be 131.7°. The second optimized structure has been labeled as *cis*-2. It differs for the relative orientation of the furan and benzothiophene rings. Since the *cis*-1 and *cis*-2 structures are asymmetric, a symmetric mirror plane produces the enantiomeric structures *σ-cis*-3 and *σ-cis*-4. The fifth minimum of the energy surface is planar (C_s point group). The associated structure has been labeled as *cis*-3.

Table 2 shows that, among the *trans* structures, there is a significant preference for the planar structures *trans*-1 and *trans*-2, with the nonplanar *trans*-3 and *trans*-4 at higher energies.

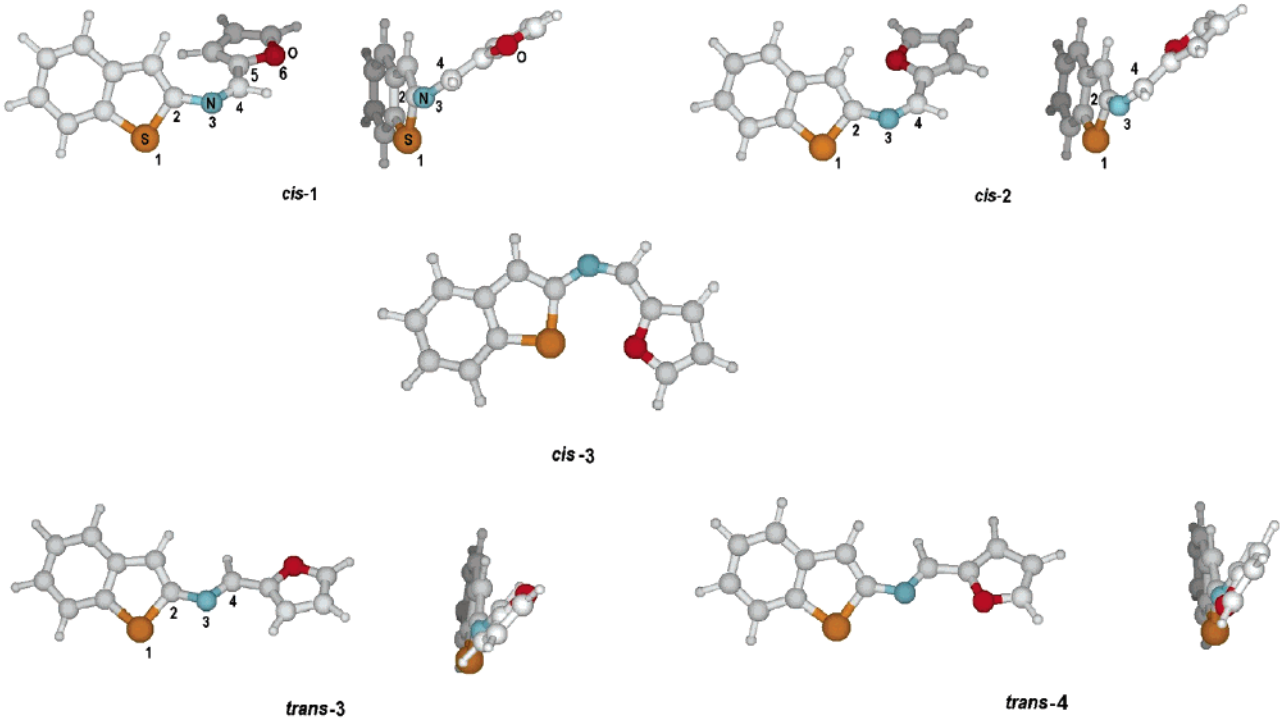

FIGURE 2. Possible conformers of the *cis* imine from furan-2-carbaldehyde and **1**.

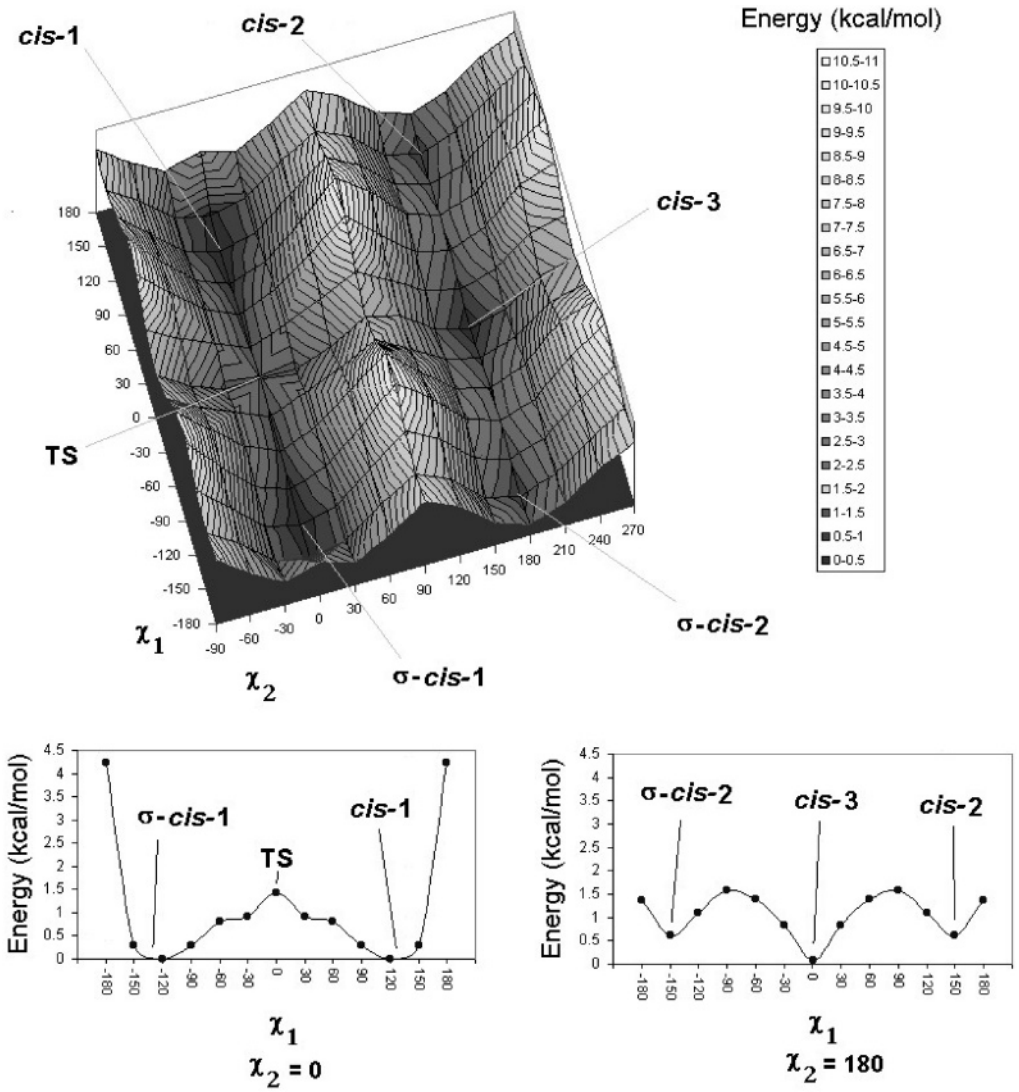

FIGURE 3. Energy map of the (χ_1,χ_2) surface; *σ-cis*-1 and *σ-cis*-2 are the enantiomers conformers of *cis*-1 and *cis*-2, respectively.

All the *cis* isomers are less stable than the *trans* isomers in terms of thermodynamic stability. According to our computation a *cis*−*trans* equilibrium should be completely displaced in favor of the *trans* isomer.

With the aim to verify if the *cis*−*trans* equilibrium can be reached, we looked for the transition structure of the *cis*−*trans* isomerization process. Its relative energy is 21.3 kcal/mol, and this value can be considered an approximation of the energy barrier from *trans* to *cis* isomer. Consequently, the inverse process (from *cis* to *trans*) can be associated to an energy barrier around 14.1 kcal/mol. The direct application of the Eyring equation leads to the prediction of the achievement of equilibrium in a few hours at ambient temperature. However, according to our experimental results, the *cis* isomer undergoes a reaction in solution phase, different from a *cis*−*trans* isomerization. This process could prevent the possibility of the *cis*−*trans* isomerization process.

According to our computations, the *cis* isomer shows very small barriers associated with the torsion angle χ_1. On the other hand, higher barriers have been found for torsion around the bond between the furan carbon atom and the iminic carbon atom (3−4−5−6 dihedral in Figure 2, named χ_2 afterward). For better describing the high internal mobility of the *cis* isomer, we have performed a relaxed energy map of the (χ_1, χ_2) surface. The values of χ_1 and χ_2 have been scanned in steps of 30° from −180° to 180° and all the other internal freedom degrees have been optimized at the B3LYP/6-31G(d) level of approximation. The resulting bidimensional energy surface is showed in Figure 3.

As is evident two low-energy paths are associated with the χ_1 torsion. Both of them accomplish a very fast interconversion between the enantiomers *cis*-1 and *σ-cis*-1 (when $\chi_2 = 0°$) and the enantiomers *cis*-2 and *σ-cis*-2 (when $\chi_2 = 180°$). In the first case, the interconversion passes through a planar ($\chi_1 = 0°$ and $\chi_2 = 0°$) transition structure (TS in Figure 3). The TS energy relative to *cis*-1 amounts to 1.4 kcal/mol. A second transition structure is predicted for $\chi_1 = 180°$, at an energy of 4.2 kcal/mol. The second reaction path ($\chi_2 = 180°$) is flatter. A planar intermediate structure ($\chi_1 = 0°$ and $\chi_2 = 180°$) is the *cis*-3 minimum, interposed between the two enantiomeric *cis*-2 and *σ-cis*-2 structures. The three transition structures (two of them are enantiomeric) show a relative energy of 1.4 and 1.6 kcal/mol. The predicted high internal mobility will be afterward used to describe the UV−vis spectroscopical data of the *cis* isomer.

Possible experimental evidence of the *cis* and *trans* isomers could come out from UV−vis spectra. Figure 4 shows the

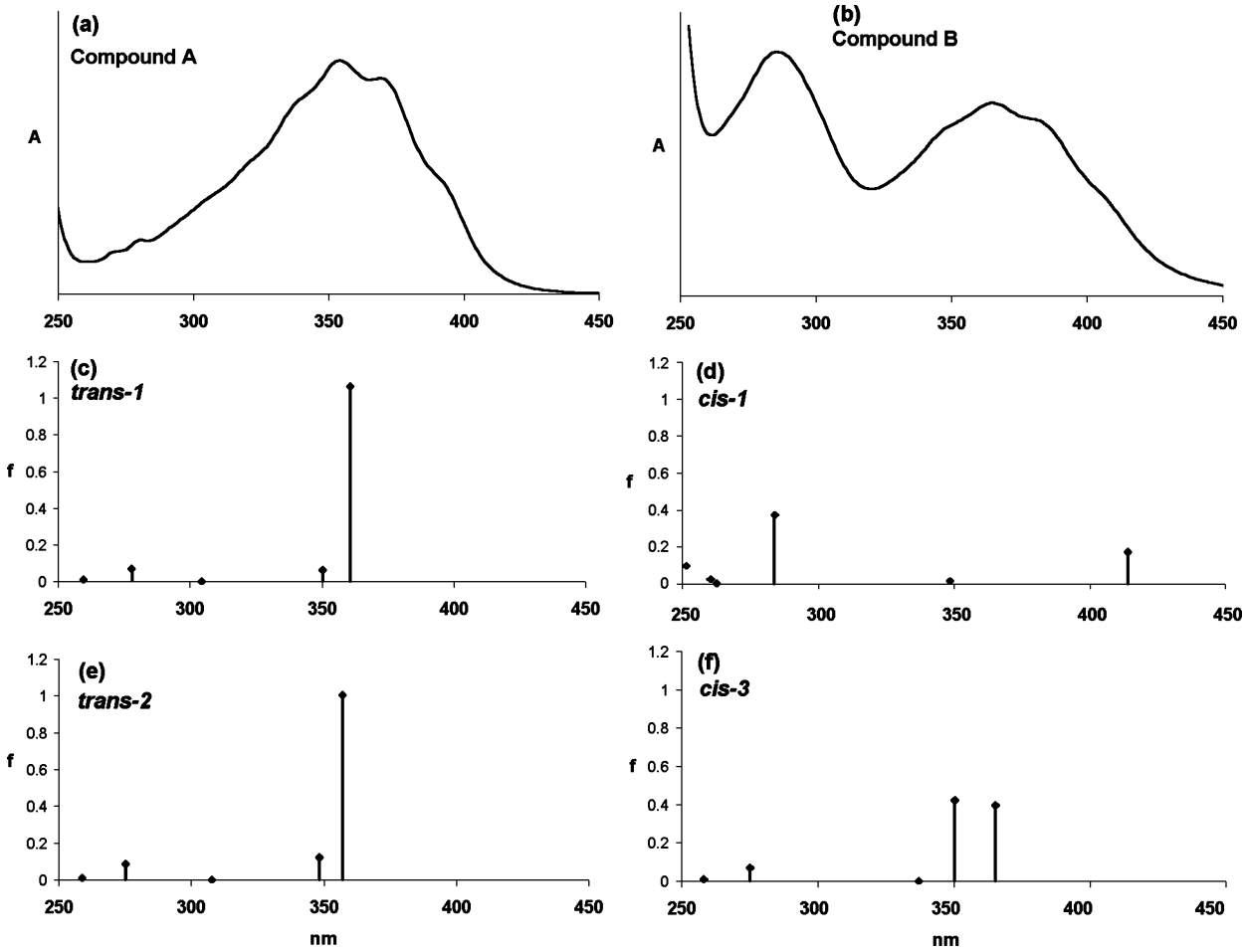

FIGURE 4. Experimental and calculated spectra of **3a** (left side) and **6a** (right side).

TABLE 3. Calculated UV−Vis Spectra of 3a (*trans*-1, *trans*-2, *trans*-3, and *trans*-4) and 6a (*cis*-1, *cis*-2, and *cis*-3)

trans-1	*trans*-2	*trans*-3	*trans*-4	*cis*-1	*cis*-2	*cis*-3
361 (1.0630)	357 (1.0056)	382 (0.5422)	381 (0.5104)	414 (0.1723)	412 (0.2508)	366 (0.3950)
350 (0.0634)	348 (0.1217)	349 (0.1568)	348 (0.1359)	349 (0.0159)	361 (0.0365)	351 (0.4217)
305 (0.0007)	308 (0.0007)	291 (0.3907)	288 (0.4343)	284 (0.3745)	286 (0.3531)	337 (0.0010)
278 (0.0696)	275 (0.0861)	269 (0.0265)	268 (0.0528)	263 (0.0024)	271 (0.0212)	275 (0.0698)
260 (0.0096)	259 (0.0119)	258 (0.0260)	258 (0.0270)	261 (0.0259)	261 (0.0196)	258 (0.0113)
245 (0.0000)	245 (0.0000)	245 (0.0131)	245 (0.0092)	252 (0.0982)	250 (0.1057)	245 (0.0180)

experimental spectra of the isolated compound A (**3a**) and compound B (**6a**) (Figure 4a,b) recorded respectively in a petroleum ether and ethyl acetate solution. In the range from 250 to 450 nm, the spectrum of **3a** is characterized by an intense absorption at 354 nm. This band shows a structure reasonably associated to a vibronic progression. Two other smaller peaks appear at about 280 and 270 nm. The spectrum of **6a** shows two main bands, with peaks at 365 and 285 nm, respectively. The band at 365 nm appears more intense, and shows a vibronic structure resembling the previous spectrum. However, in comparison, it is significantly broader and light absorption can be easily observed until 450 nm. The band at 285 nm presents a higher peak absorbance, as a possible consequence of overlap with the intense absorption below 250 nm (not recorded) and the tail of the first band at 365 nm.

Parts c and e in Figure 4 show the computed spectra of the two most stable *trans* isomers (*trans*-1 and *trans*-2). Vertical transition wavelengths and oscillator strengths are reported for all the transitions from 250 and 450 nm. Table 3 collects the same information. The computed spectra are characterized by an intense absorption at 361 and 357 nm for the *trans*-1 and *trans*-2 structures, respectively (Table 3). No other absorptions of comparable intensity have been predicted, hence, the agreement with the experimental spectrum can be considered good. Furthermore, the experimental weak peaks at 280 and 270 nm can be associated with the computed transitions at 278 and 260 nm for the *trans*-1 isomer. Alternatively, the same peaks could be associated with a vibronic progression assigned to the computed absorption at 278 nm because of its higher oscillator strength. The same conclusion can be extended to the *trans*-2 isomer, which shows two similar relatively weak transitions computed at 275 and 259 nm, respectively.

According to the computed excited-state composition, the first intense transition can be considered a HOMO-LUMO excitation. Figure 5a shows these two Kohn−Sham orbitals for the *trans*-1 isomer (the *trans*-2 isomer orbitals have not been reported because they are very similar). It is possible to note that the HOMO and LUMO have a significantly different nodal pattern,

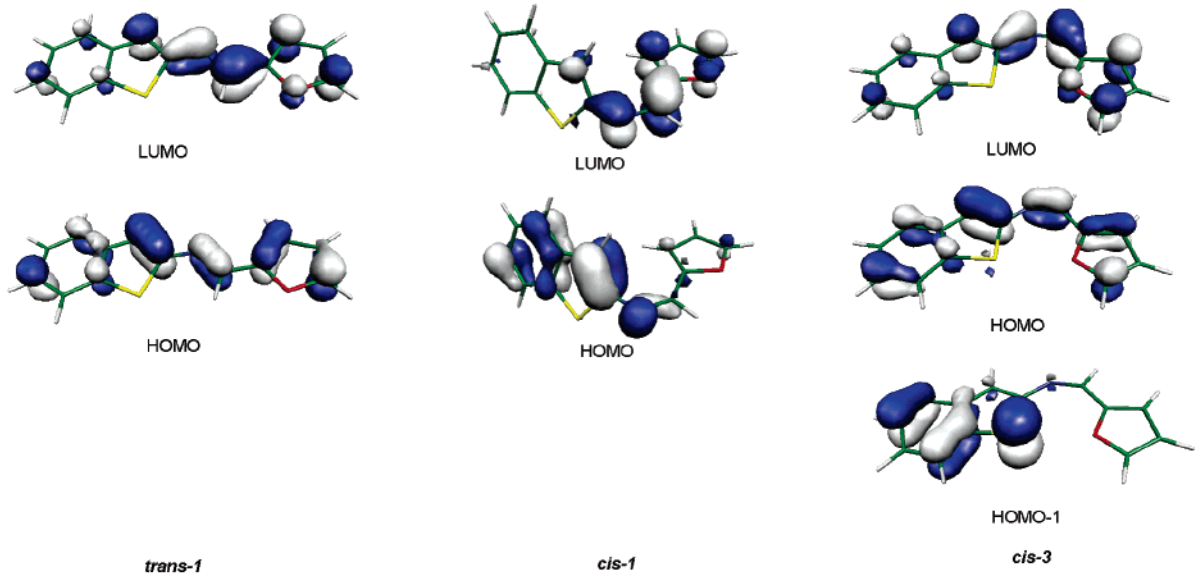

FIGURE 5. Kohn−Sham orbitals of **3a** (*trans*-1) and **6a** (*cis*-1 and *cis*-3).

TABLE 4. Decomposition of the Absorption Spectrum of 3a

curve	peak wavelength (nm)	fwhm (nm)	relative peak height
1	400	40.7	0.104
2	391	20.9	0.429
3	372	20.1	0.930
4	354	19.4	1.000
5	337	19.0	0.765
6	321	19.1	0.507
7	304	20.3	0.319
8	289	27.6	0.272
9	279	6.2	0.058
10	271	10.9	0.122
11	260	11.9	0.118
12	236	19.8	1.539

which allows the prediction of a large geometry deformation in the excited state, which should involve both the iminic bridge and the aromatic rings. This is in agreement with the extended vibronic structure observed in the experimental spectrum.

A decomposition of the experimental spectrum of compound **3a** has then been performed. A set of 12 Gaussian curves have been used, by fitting their peak wavelength, broadness (precisely full width at half-maximum, fwhm), and peak height. The characteristic parameters of the curves have been listed in Table 4, where the curves have been numbered in order of decreasing peak wavelength. Figure 6 is intended to give a graphical description. The reference curve for the reported peak height is the Gaussian curve 4, the one corresponding to the maximum of the experimental first absorption band.

Curves 2 to 7 show similar fwhm, and have been chosen to describe the vibronic structure of the band. Curve 1 is broader, probably to better describe the band extension at longer wavelength.

Curve 8 is aimed to take into account the long tail of the band, and curves 11 and 12 allow a good fitting of the steep absorption from 255 nm to shorter wavelength. Curves 9 and 10 describe the two small peaks at about 280 and 270 nm. Energy gaps between adjacent curves from 2 to 7 extend from 1302 cm^{-1} (19 nm from curve 2 to curve 3) to 1604 cm^{-1} (17 nm from curve 6 to curve 7). Separations around curve 4 (the peak of the band) are 1371 cm^{-1} between curve 3 and curve 4 (18 nm) and 1425 cm^{-1} between curve 4 and curve 5 (17 nm). Computed normal modes and relative vibrational frequencies of the *trans*-1 show that the value found above can be associated to bond stretching motions distributed in the backbone of the molecule. They involve both the iminic bridge and the aromatic rings.

Unlike the *trans* isomer, the computational prediction of the *cis* isomer spectrum appears less straightforward. As abobe reported in Table 2, there exist several minima of the energy surface that can be assigned to the *cis* isomer, and all of them are very close in energy. The structures *cis*-1 and *cis*-2 (Figure 2) present almost coincident computed electronic spectra, as reported in Table 3. In both cases, the computed spectrum shows two main features. For the *cis*-1 structure, the first one is located at 414 nm and the second one at 284 nm. For the *cis*-2 structure, the first feature is located at 412 nm and the second one at 286 nm. The second transition is computed somewhat more intensely. Figure 4d is a schematic representation of the *cis*-1 computed spectrum. Unlike the *trans* isomers, they present two predominant absorptions, consistent with the two absorption bands of the compound B spectrum (Figure 4b). A particularly good agreement can be observed for the position of the second intense band at 280 nm. On the contrary, the first experimental absorption band is located at 364 nm, whereas the computational one is at about 414 nm. A similar large computational difference has not been observed for the *trans* isomer. Furthermore, such an error only affects the first band of the compound B spectrum.

As reported above, the first band presents a vibronic structure that is very similar to the compound A spectrum, assigned to the *trans* isomer. A possible explanation would be the existence of a *trans* and *cis* isomer mixture. Consequently, the *cis* isomer spectrum can be obtained by subtracting the experimental spectrum (compound B, Figure 4) by a properly scaled spectrum of compound A. In this light, we have performed a decomposition of the compound B spectrum in terms of the compound A spectrum and two Gaussian curves which describe the absorption at about 280 nm and the longer tail at wavelengths longer than 400 nm. Figure 7 shows the results of this work. It is clear that the vibronic structures of the experimental and fitted spectrum do not coincide, and no good fit could be obtained by the

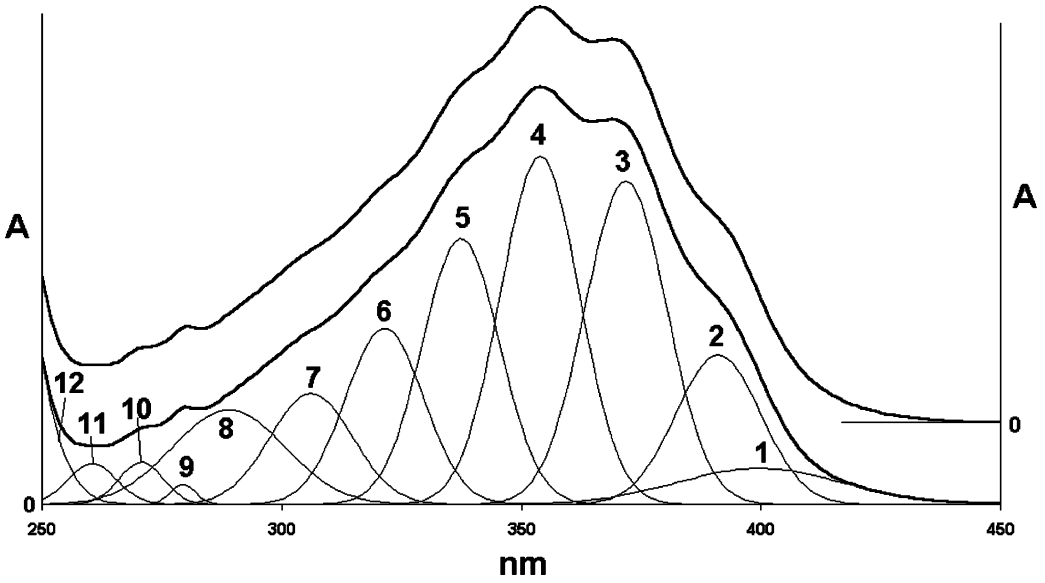

FIGURE 6. Decomposition of the UV−vis spectrum of **3a**. The Gaussian curves have been labeled with numbers from 1 to 12 for reference in Table 4

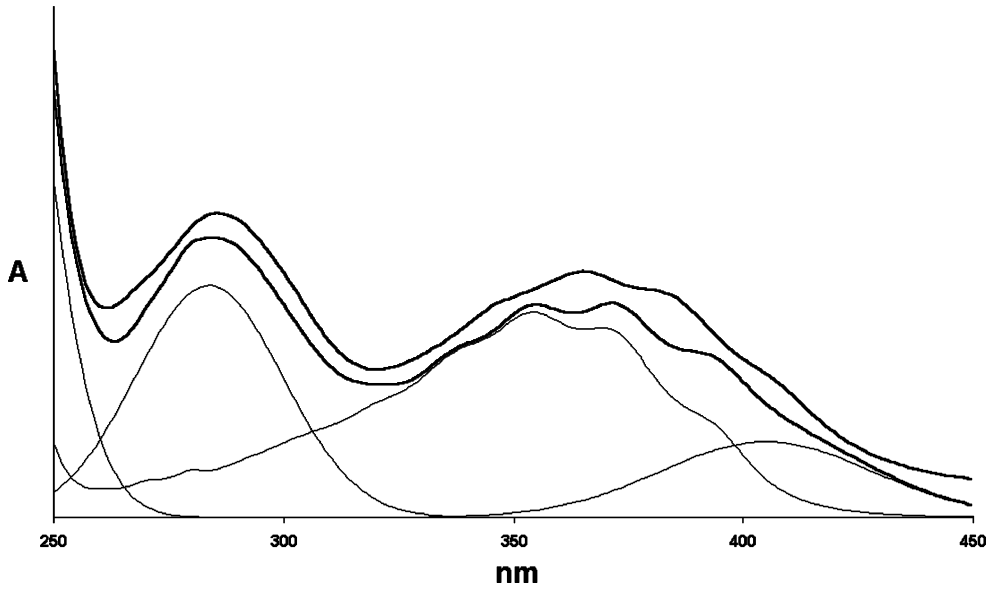

FIGURE 7. First attempted decomposition of the absorption spectrum of **6a**.

combination of the compound A vibronic structure and the two Gaussian curves. Thus, according to our conclusion, we can reasonably exclude the presence of the *trans* isomer.

According to DFT computations, the *cis*-3 structure has the same energy as the *cis*-1 structure, thus it can be populated in a consistent way. Its computed spectrum shows two main absorptions at 366 and 351 nm. Their intensities are similar and their sum is larger than all the other excitations until 250 nm. Furthermore, they reasonably merge to form a single intense band. The resulting predicted spectrum should be similar to the *trans*-1 and *trans*-2 spectra, which are planar like the *cis*-3 structure. Figure 5 shows the HOMO, HOMO-1, and LUMO computed orbitals for the *cis*-3 structure. It is evident how the HOMO and LUMO are similar to the *trans*-1 homologues, apart from the obvious difference due to the isomeric structure. Thus, monoelectron excitation from the HOMO to the LUMO should lead to a vibronic structure that should be similar to the *trans*-1 structure. The first computed transition is mostly associated with the HOMO-LUMO monoelectronic transition, with an important but smaller contribution from the excitation from the HOMO-1 to the LUMO (Table 5).

TABLE 5. Selected Computed Transitions in 6a

state	energy (nm)	oscillator strength	composition
S_1	366	0.3950	HOMO-LUMO −0.37190 HOMO-1-LUMO 0.52980
S_2	351	0.4217	HOMO-LUMO 0.56860 HOMO-1-LUMO 0.32081

The same monoelectronic contributions are substantially inverted in the case of the second computed transitions. Thus, there is the possibility that the evident vibronic structure of the *trans*-1 HOMO-LUMO transition is still present in the case of the *cis*-3 structure.

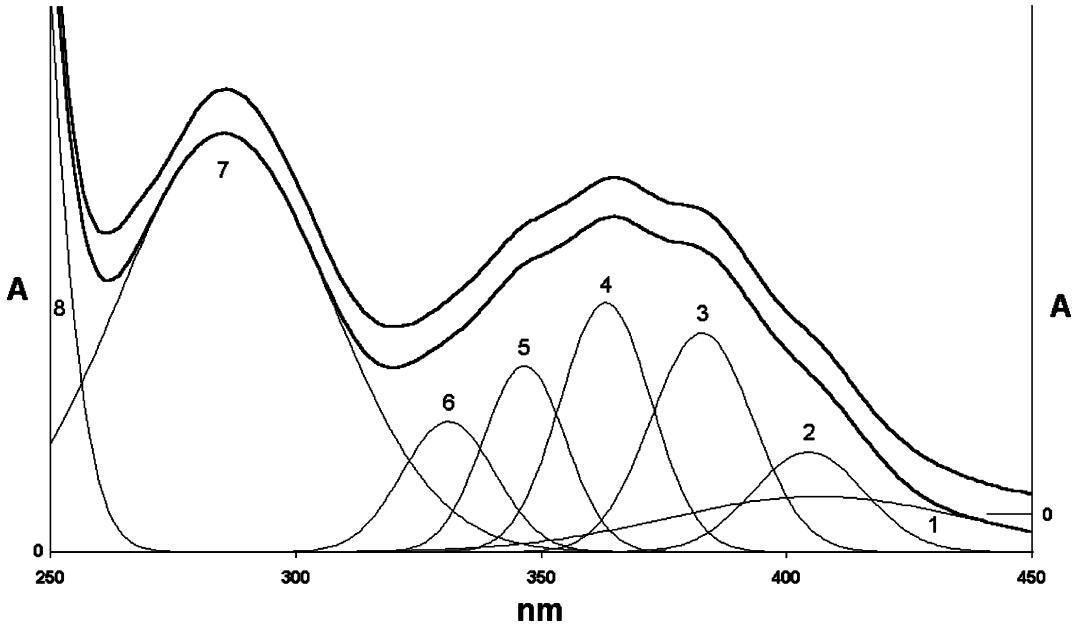

FIGURE 8. Decomposition of the absorption spectrum of **6a**. The used Gaussian curves have been labeled with numbers from 1 to 8 for reference in Table 5

TABLE 6. Decomposition of the Absorption Spectrum of 6a

curve	peak wavelength (nm)	fwhm (nm)	relative peak eight
1	406	72.8	0.133
2	405	26.7	0.239
3	383	24.5	0.523
4	363	21.8	0.596
5	346	19.7	0.446
6	331	22.2	0.312
7	286	50.8	1.000
8	237	22.1	3.744

However, the *cis*-3 structure alone cannot describe the intense experimental absorption at about 280 nm. As said above, only the nonplanar *cis* structures predict this band absorption.

We can conclude that the experimental spectrum is the consequence of similar populations of the planar *cis* structure (*cis*-3) and tilted *cis* structures (*cis*-1, *cis*-2 and their enantiomers).

With the aim to further confirm this hypothesis, we have performed a decomposition of the compound **6a** spectrum in terms of 8 Gaussian curves, similar to the case of the *trans* isomer. Figure 8 shows our results and Table 6 collects the parameters of the Gaussian curves ordered by decreasing peak wavelength.

Gaussian curve 8 is used to fit the portion of the spectrum at about 250 nm, accordingly we will not consider it. Gaussian curves from 2 to 6 describe the vibronic structure of the observed first band. Curve 1 is broad and relatively flat to fit the extended band tail at longer wavelengths. Its peak wavelength is placed at 414 nm. Curve 7 is the most intense Gaussian curve, with maximum at 285 nm. As a consequence, curves 1 and 7 can be associated with the computed absorption at 414 and 284 nm for the *cis*-1 structure, and/or 412 and 286 nm for the *cis*-2 structure. The broad character of curve 1 is not surprising if we consider that it is associated with the HOMO-LUMO transition whose characteristics are similar to those of the *trans*-1 structure. Figure 5 shows the HOMO and LUMO of the *cis*-1 structure. The nodal pattern of the LUMO transition is similar to the case of the *trans* structure, and the HOMO differs for the lower contribution from the furan ring.

The observed difference in the absorption spectra of the planar *cis*-3 and nonplanar *cis* structures required a deeper understanding of the relationship between the χ_1 twist angle and the absorption spectra. This investigation has been performed on the low-energy isomerization path associated with $\chi_2 = 0°$. For each of the energy minimized structures with torsion angle χ_1 from 0 to 150° a TD-DFT computation has been performed. The resulting computed spectra are reported in Figure 9.

The structure at $\chi_1 = 180°$ has not been considered because of its higher energy and consequent lower accessibility at ambient temperature. The structures with negative χ_1 are the enantiomeric image of the structures reported in Figure 2, thus their computed spectra are the same. The structure associated with $\chi_1 = 0°$ is the TS structure in Figure 3. It is planar, and its spectrum is similar to the spectra described for the *cis*-3 and *trans*-1 structures; no intense absorption is present at about 280 nm, while the first intense band is computed at about 360 nm. On the other hand, all the titled structures show an intense absorption at about 280 nm and a further absorption band over 400 nm. It is evident that a χ_1 value of 30°, a relatively small deformation from planarity, is sufficient to induce the transition from one (the *trans*-like spectrum) to the other kind of spectrum.

We can conclude that the presence of the absorption at about 280 nm is diagnostic of tilted structures, whereas the presence of the intense band at about 360 nm with vibronic structure is diagnostic of planar structures. In the case of the *trans* isomer, the energy surface favors the planar structures. As a consequence, the spectrum is well reproduced by computations on the most stable *trans*-1 structure, which is planar, as well as computations on the equally planar *trans*-2 structure. In the case of the *cis* isomer, both planar structures (like the *cis*-3 structure) and tilted structures (like the *cis*-1 and *cis*-2 structures and their enantiomers) are populated. The experimental spectrum results from the combination of the typical planar-structures spectrum

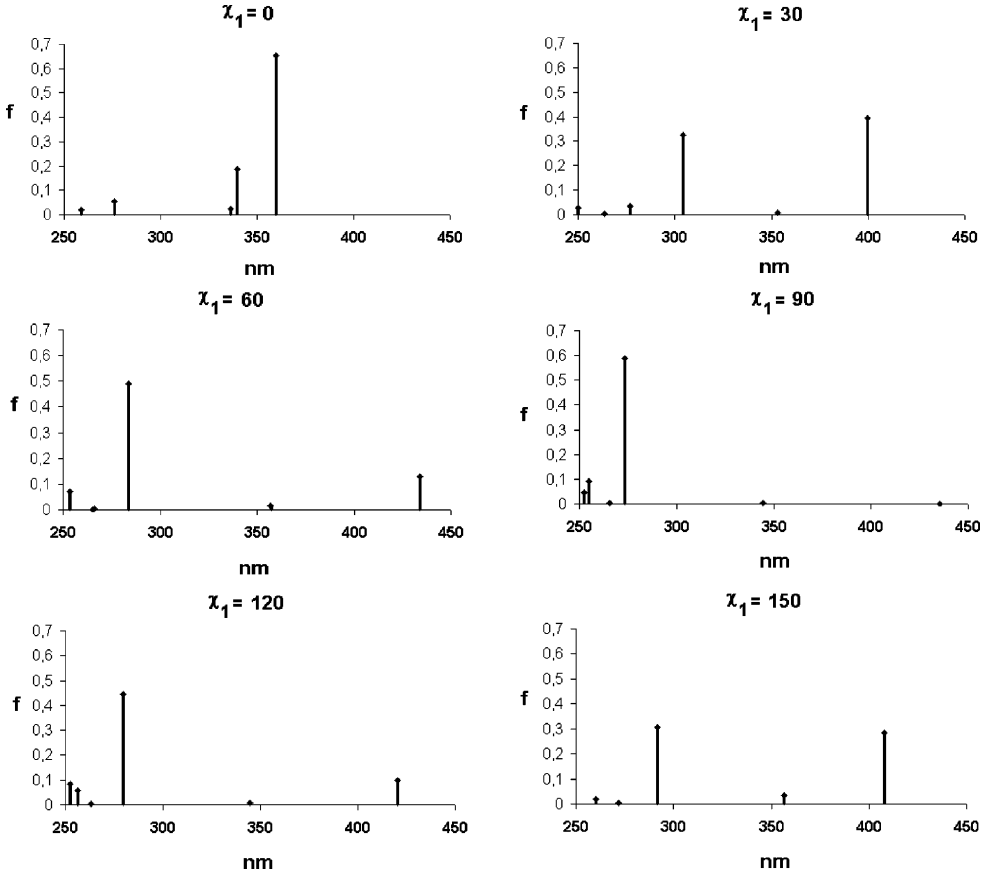

FIGURE 9. Calculated absorption spectra of **4a** at different χ_1 values.

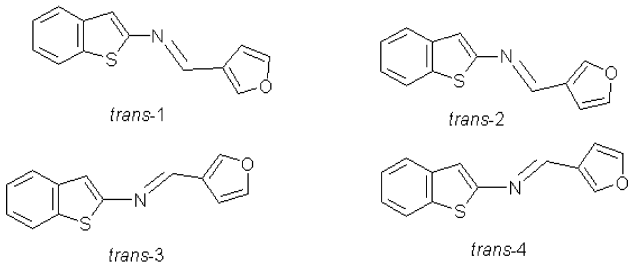

FIGURE 10. Possible conformers of the imines obtained in the reaction between furan-3-carbaldehyde and **1**.

and the typical tilted-structures spectrum and both of them must be considered for a correct assignment.

Determination of *Cis*−*Trans* Configuration of Imines. The computations performed on the imines obtained starting from **2a** have been equally applied to the imines obtained from **2b**, **4a**, **4b**, **2c**, and **2d**.

Studies about the energy surface at the B3LYP/6-31G(d) level of approximation confirmed that the *trans* isomers are significantly more stable than the *cis* isomers. Furthermore, in all the cases, four minima of the reaction surface can be assigned to the *trans* isomers. Figure 1 above, associated with the imines obtained from furan-2-carbaldehyde, has been equally used for naming the *trans* isomers of the imines obtained from thiophene-2-carbaldehyde, 5-nitrothiophene-2-carbaldehyde, and 5-nitrofuran-2-carbaldehyde. For the imines obtained from thiophene-3-carbaldehyde and furan-3-carbaldehyde, the chosen nomenclature is shown in Figure 10 for the imines obtained from furan-3-carbaldehyde.

TABLE 7. Structures Obtained for the Imines Deriving from Thiophene-2-carbaldehyde, Furan-3-carbaldehyde, Thiophene-3-carbaldehyde, 5-Nitrofuran-2-carbaldehyde, and 5-Nitrothiophene-2-carbaldehyde and the Energy of the Reaction Surface Points Associated with the Optimized Structures[a]

	heteroaromatic substituent				
isomer	2-thienyl	3-furyl	3-thienyl	5-nitro-2-furyl	5-nitro-2-thienyl
trans-1	1.7 (C_s)	0.0 (C_s)	1.0 (C_s)	0.0 (C_s)	1.6 (C_s)
trans-2	0.0 (C_s)	1.0 (C_s)	0.0 (C_s)	1.5 (C_s)	0.0 (C_s)
trans-3	4.2 (C_1)	2.4 (C_1)	2.5 (C_1)	7.9 (C_1)	4.5 (C_1)
trans-4	2.6 (C_1)	3.4 (C_1)	3.5 (C_1)	4.8 (C_1)	3.0 (C_1)
cis-1	9.7 (C_1)	7.5 (C_1)	8.4 (C_1)	8.6 (C_1)	11.0 (C_1)
cis-2	8.7 (C_1)	8.0 (C_1)	9.0 (C_1)	8.0 (C_s)	10.0 (C_1)
cis-3	none	none	none	7.9 (C_s)	none
cis-4	10.3 (C_1)	none	none	8.7 (C_1)	10.9 (C_1)

[a] The point groups of the reported structures have been included in parentheses for distinguishing the planar structures from the nonplanar ones.

Table 7 collects the structures found for all the compounds, and the energy of the reaction surface point associated with the optimized structures.

As in the case of the imines obtained from **2a**, we found that the *trans* isomers are more stable than the *cis* isomers. In particular, the planar *trans* isomers (point group C_s in Table 7) are the most stable structures. The major difference found worthy of note was that the *trans*-1 isomer is the most stable in the imines obtained from **4a** and **2c** (and also **2a**), whereas *trans*-2 is the most stable structure in the imines obtained from **2b**, **4b**, and **2d**.

As for the imines obtained from **2a**, the other *cis* isomers are associated with a more complex potential surface. Also in

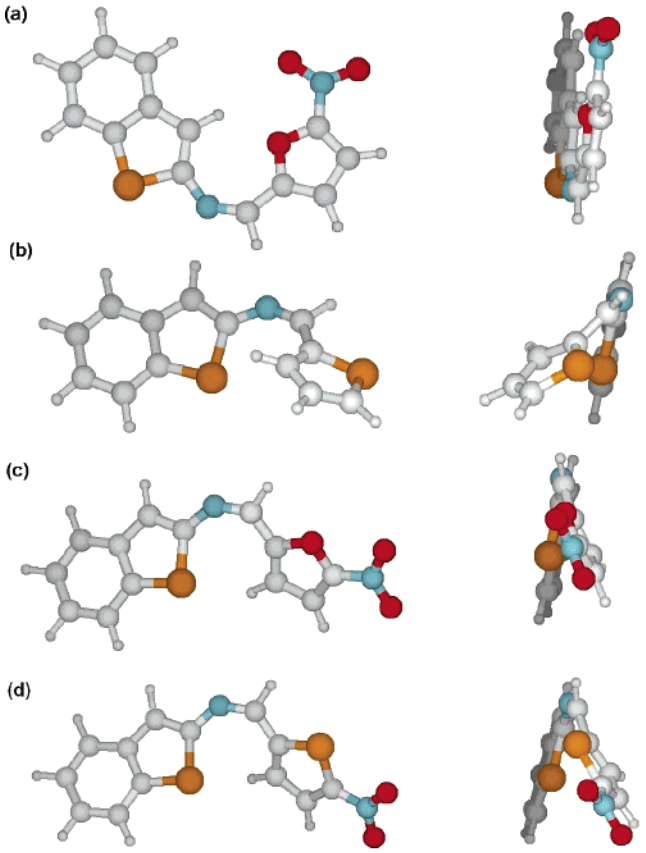

FIGURE 11. The computed *cis*-2 structure for the imine obtained from 5-nitrofuran-2-carbaldehyde (a), and computed *cis*-4 structures of the imines obtained starting from thiophene-2-carbaldehyde (b), 5-nitrofuran-2-carbaldehyde (c), and 5-nitrothiophene-2-carbaldehyde (d).

this case, the rotation of the benzothiophene ring with respect to the iminic function appears more facile in comparison to the rotation of the furyl or thienyl rings. The nonplanar (C_1 point group) *cis* structures analogue to the *cis*-1 and *cis*-2 structures of Figure 2 have been found in all the cases apart from the imine obtained from **2c**, where a planar structure replaces the *cis*-2 structure (this structure is still labeled as *cis*-2 in Table 7 and it is showed in Figure 11). This planar structure analogue to the *cis*-3 structure of Figure 2 can be found only in the imine from **2c** and it appears more stable than the nonplanar analogous ones. New *cis* minima can be found in the imines obtained from **2b**, **2c**, and **2d**. All of them are labeled as *cis*-4, but in the case of the imine obtained from **2b** this structure strongly differs from the *cis*-4 structures of the imines obtained from **2c** and **2d**. Figure 11 is intended to give a graphical description of the *cis*-4 structures.

Table 8 collects some computed excitation energies and oscillator strengths for the most significant structures of the imines obtained from **2b**, **4a**, and **4b**. As evidenced below, the presence of the NO_2 group completely changes the absorption spectra of the compounds. Thus, the imines obtained from **2c** and **2d** will be treated in a following paragraph.

From Table 8, we can observe that the *trans*-2 structure of the imine obtained from **2b** shows an absorption spectrum that is similar to the one described for the imine obtained from **2a**. The spectrum is characterized by an intense band located at 371 nm, and no other features have been found of similar intensity. A possible difference can be due to the presence of a relatively intense transition at 272 nm (S_5), whose oscillator strength is about eight time smaller in comparison to the first absorption band (S_1). A similarly intense absorption band has not been found in the imine obtained from **2a**.

Two compounds have been isolated in the reaction of **1** with **2b**. The first one shows an experimental spectrum in good agreement with the computed *trans*-1 spectrum. The recorded spectrum shows an intense absorption band with a vibronic structure whose peak is placed at 364 nm (in hexanes and ethyl acetate). A second, weaker band is formed by two equally intense peaks at 280 and 272 nm. More problematic has been the assignment of the second isolated fraction. In hexanes−ethyl acetate mixture, its spectrum shows an intense band at 377 nm with a similar pattern in comparison to the first structure. As for compound **6a** (Figure 4), assigned to the *cis* isomer, this band appears red-shifted and broader. Furthermore, additional intense bands have been observed at about 278 and 256 nm. According to Table 8, the computed spectrum of the most stable *cis*-2 structure shows two intense peaks at 284 and 260 nm which have a good match with the experimental second and third absorption peaks. However, the band at 377 nm is not predicted; the first intense computed band is located at 439 nm. As discussed in the case of the imine obtained from **2a**, a single structure is not capable of reproducing the spectrum of the second obtained compound. Furthermore, also in this case, computations on the nonplanar structure seem to correctly

TABLE 8. Calculated Absorption Spectra of the Imines Obtained from Thiophene-2-carbaldehyde, Furan-3-carbaldehyde, and Thiophene-3-carbaldehyde

2-thienyl[a]		3-furyl[a]		3-thienyl[a]	
trans-2		*trans*-1		*trans*-1	
S_1	371 nm (0.9325)	S_1	336 nm (0.3965)	S_1	344 nm (0.7416)
S_2	356 nm (0.0749)	S_2	331 nm (0.5881)	S_2	338 nm (0.3469)
S_3	307 nm (0.0005)	S_3	296 nm (0.0007)	S_3	300 nm (0.0006)
S_4	285 nm (0.0336)	S_4	283 nm (0.0075)	S_4	285 nm (0.0119)
S_5	272 nm (0.1192)	S_5	255 nm (0.0103)	S_5	264 nm (0.0766)
S_6	260 nm (0.0062)			S_6	255 nm (0.0106)
cis-2		*cis*-1		*cis*-1	
S_1	439 nm (0.0902)	S_1	380 nm (0.1590)	S_1	397 nm (0.1576)
S_2	360 nm (0.0117)	S_2	324 nm (0.0125)	S_2	333 nm (0.0087)
S_3	284 nm (0.2699)	S_3	270 nm (0.2423)	S_3	286 nm (0.0725)
S_4	265 nm (0.0198)	S_4	261 nm (0.0013)	S_4	264 nm (0.0470)
S_5	263 nm (0.0330)	S_5	256 nm (0.0308)	S_5	263 nm (0.2820)
S_6	260 nm (0.2220)			S_6	253 nm (0.0223)
S_7	253 nm (0.0599)				

[a] Heteroaromatic substituent.

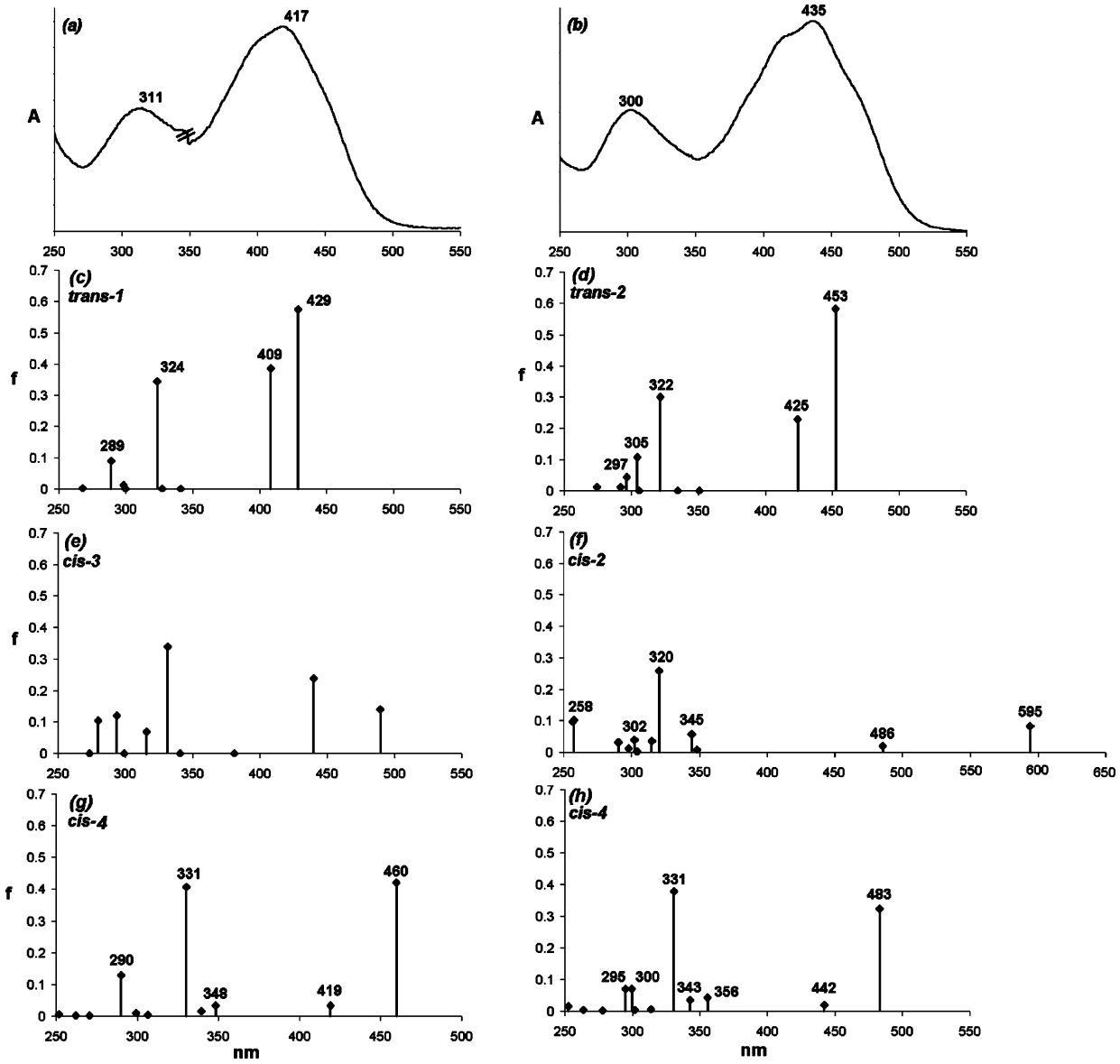

FIGURE 12. Experimental and calculated spectra of **2c** (left side) and **2d** (right side).

describe the peaks at wavelengths under 300 nm, but fail to reproduce the first absorption band. In the case of the imine obtained from **2a**, the planar *cis*-3 structure allows the justification of the first experimental band. The same is true for **2b**. The planar (*cis*-3) structure is associated with computed transitions at 372 and 347 nm with oscillator strengths of 0.4974 and 0.2451, respectively. No other transitions have been predicted with similar oscillator strength. Thus, also in this case, the second fraction spectrum is compatible with the presence of planar and nonplanar *cis* structures. Unfortunately, in the case of the imine obtained from **2b** the *cis*-3 structure is not a minimum on the B3LYP/6-31G(d) energy surface, but it is associated with a transition structure (saddle point) at 3.1 kcal/mol respective to the *cis*-2 structure. This energy is not compatible with a significant population of the planar structure at room temperature. At the BLYP/6-31G(d) level of approximation, the energy difference is reduced to 1.7 kcal/mol. The Maxwell−Boltzmann equation would predict a population of this fraction of about 6%. This amount allows the observation of the first two bands of the *cis*-3 (planar) structure by virtue of their large oscillator strength. On the contrary, Hartree−Fock computations with the same basis set describe an energy gap beyond 7.0 kcal/mol in favor of the nonplanar structure. It appears clear that the different method of computing the correlation-exchange energies significantly affects the relative energies of planar and nonplanar structures. We have noted a possible correlation between the bond angles around the nitrogen and carbon atoms of the iminic function and the energy preference for the nonplanar structures. If a computational model allows the achievement of larger angles without great energy loss, then a larger distance is observed between the two aromatic rings. The consequent lower steric hindrance allows a larger energy stability of the planar structure. In other words, if a computational model strongly forces the nitrogen and carbon atoms of the iminic bridge to be sp^2-hybridized, then the distance between the two aromatic rings is shorter, with consequent destabilization. This is the case for the Harteree−Fock approach. On the contrary, the BLYP approach seems to favor larger bond angles, so that the repulsive steric interaction between the aromatic rings is lowered. The B3LYP (which contains both

the Hartree−Fock exchange and the LYP exchange) is somewhat intermediate.

This computational issue is actually under investigation in our laboratories, with the aim to understand the origin of the discrepancies among the different computational models.

Determination of the *Cis*−*Trans* Configuration of Imines from 2c and 2d. Similar considerations can be applied to the imines obtained from both **4a** and **4b**. Also in this case, the first isolated compound shows a spectrum in very good agreement with the most stable planar *trans* structures. The second isolated compound, on the contrary, presents a spectrum that would be well described as resulting from a mixture of planar and nonplanar structures.

Figure 12 collects the experimental spectra recorded for the imines obtained from both **2c** (**3c**) (Figure 12a) and **2d** (**3d**) (Figure 12b) together with computed spectra for some optimized structures whose energy is reported in Table 7. The experimental spectrum of **3c** shows two intense bands at 417 and 311 nm. Computed spectra for the most stable *trans*-1 structure and *cis*-3 and *cis*-4 structures are reported. The *trans*-2 computed transition wavelengths and oscillator strengths are very close to the *trans*-1 ones, thus it has not been shown. *trans*-3 and *trans*-4 computed spectra show similar characteristics, but the first absorption band is red shifted by about 20 nm. *cis*-1 and *cis*-2 structures are associated with similar spectra in comparison to the *cis*-3 one and they also have been neglected. As is evident, the *trans*-1 structure (indeed also the other *trans*-2 structures) shows the best agreement with the experimental spectrum, both in terms of predicted peak wavelengths and in terms of relative peak intensities. In this light, we can assign the isolated compound to the *trans* isomer with good confidence.

A similar discussion can be applied to the imine **3d**. The experimental spectrum shows two intense features at 435 and 300 nm. Figure 12 reports the computed spectra of the *trans*-2 spectrum and the most stable *cis* structures. Also in this case, the other *trans* structures produced similar spectra. The not reported *cis*-1 structure shows a very similar absorption pattern in comparison to the *cis*-2 structure. The *trans*-2 isomer (the most stable structure) shows the best agreement with the experimental spectrum. The conclusion of our computations is therefore that the *trans* isomer is the main product of the reaction.

Conclusion

In conclusion we have shown that the Staudinger reaction can be used for the synthesis of new imines from the coupling between 2-benzothienyldiphenylmethyliminophosphorane and heterocyclic aldehydes. The reaction at 60 °C gave the formation of only the *trans* isomer while, by using a higher temperature, also the *cis* isomer can be isolated. The *cis* isomers were the only compounds showing a photochemical reactivity to give the corresponding condensed pyridine derivatives.

An exhaustive theoretical evaluation of the UV−vis spectra of the obtained imines **3**, **5**, **6**, and **7** allowed us to assign *cis* or *trans* stereochemistry to the synthesized imines. This reported approach, based on experimental and theoretical considerations, represents the first *cis*−*trans* configuration assignment based on UV−vis absorption spectra.

In this paper, we have also limited our discussion on the possibility that our computations could fail in predicting the energy difference between planar and nonplanar structures, since it is generally difficult to correctly compute small energy differences, especially if they arise from subtle electron correlation effects. Furthermore, we have to consider that the experimental data have been collected in solution phase, where interaction with the solvent can change the relative stability. However, we can undoubtedly assert that B3LYP, BLYP, and CIS computations (configuration interaction based on single excitations performed on HF/6-31G(d) geometry) agree in describing similar spectra for *cis* and *trans* planar structures, and different spectra for nonplanar and planar *cis* structures.

Experimental Section

2-[*N*-(2-Furylideneamino)]benzo[*b*]thiophene (3a). A 50.0 mg (0.14 mmol) sample of iminophosphorane **1** and 11.9 μL (0.141 mmol) of furan-2-carbaldehyde in dry toluene (3 mL) were stirred at 60 °C in N_2 atmosphere for 22 h. After solvent removal in vacuo the crude mixture was purified on silica gel with a 8:2 mixture of petroleum ether and ethyl acetate. Compound **3a**, 17.0 mg (53% yield) of yellow powder at R_f 0.70, was obtained; mp 90 °C. ^{1}H NMR (500 MHz, $CDCl_3$) δ 8.30 (s, 1 H), 7.74−7.72 (m, 2 H), 7.67 (d, 1 H, J = 1.5 Hz), 7.41 (s, 1 H), 7.30−7.38 (m, 2 H), 7.03 (d, 1 H, J = 3.5 Hz), and 6.62−6.60 ppm (m, 1H); ^{13}C NMR (125 MHz, $CDCl_3$) : 153.8, 146.6, 139.2, 136.5, 131.2, 129.1, 125.7, 125.0, 124.3, 122.8, 122.2, 117.6, and 112.9 ppm; MS, *m*/*z*, 227 (M^+). Anal. Calcd for $C_{13}H_9NOS$: C, 68.70; H, 3.99. Found: C, 68.82; H, 3.80.

2-[*N*-(2-Thienylideneamino)]benzo[*b*]thiophene (3b). A 49.3 mg (0.142 mmol) sample of iminophosphorane **1** and 13.2 μL (0.141 mmol) of thiophene-2-carbaldehyde in dry toluene (3 mL) were stirred at 60 °C in N_2 atmosphere for 24 h. After solvent removal in vacuo the crude mixture was purified on silica gel with a 8:2 mixture of hexanes and ethyl acetate. Compound **3b**, 32.7 mg (84% yield) of yellow powder at R_f 0.78, was obtained; mp 135−138 °C. ^{1}H NMR (300 MHz, $CDCl_3$) δ 8.59 (s, 1 H), 7.75−7.67 (m, 2 H), 7.57−7.50 (m, 2 H), 7.37−7.29 (m, 3 H), and 7.18−7.13 ppm (m, 1 H); ^{13}C NMR (75 MHz, $CDCl_3$) δ 151.3, 142.3, 139.0, 132.3, 131.0, 130.6, 129.6, 128.0, 125.3, 124.6, 124.0, 122.6, and 121.0 ppm. Anal. Calcd for $C_{13}H_9NS_2$: C, 64.16; H, 3.73. Found: C, 64.10; H, 3.67.

2-[*N*-(3-Furylideneamino)]benzo[*b*]thiophene (5a). A 50.0 mg (0.14 mmol) sample of iminophosphorane **1** and 11.9 μL (0.141 mmol) of furan-3-carbaldehyde in dry toluene (3 mL) were stirred at 60 °C in N_2 atmosphere for 22 h. After solvent removal in vacuo the crude mixture was purified on silica gel with a 8:2 mixture of hexanes and ethyl acetate. Compound **5a**, 17.2 mg (54% yield) of yellow powder at R_f 0.86, was obtained; mp 70 °C. ^{1}H NMR (500 MHz, $CDCl_3$) δ 8.47 (s, 1 H), 7.94 (s, 1 H), 7.77−7.71 (m, 2 H), 7.53 (s, 1 H), 7.37−7.30 (m, 3 H), and 6.98 ppm (d, 1 H, J = 1.5 Hz); ^{13}C NMR (125 MHz, $CDCl_3$) δ 154.4, 151.0, 144.8, 139.4, 136.4, 131.2, 129.1, 125.4, 125.0, 124.1, 122.9, 120.9, and 108.2 ppm; MS, *m*/*z*, 227 (M^+). Anal. Calcd for $C_{13}H_9NOS$: C, 68.70; H, 3.99. Found: C, 68.63; H, 4.08.

2-[*N*-(3-Thienylideneamino)]benzo[*b*]thiophene (5b). A 47.6 mg (0.137 mmol) sample of iminophosphorane **1** and 12.0 μL (0.137 mmol) of thiophene-3-carbaldehyde in dry toluene (3 mL) were stirred at 60 °C in N_2 atmosphere for 24 h. After solvent removal in vacuo the crude mixture was purified on silica gel with a 8:2 mixture of hexanes and ethyl acetate. Compound **5b**, 17.8 mg (53% yield) of yellow powder R_f 0.78, was obtained; mp 123−126 °C. ^{1}H NMR (300 MHz, $CDCl_3$) δ 8.52 (s, 1 H), 7.84 (d, 1 H, J = 1.92 Hz), 7.76−7.69 (m, 3 H), 7.42−7.39 (m, 1 H), and 7.36−7.31 ppm (m, 3 H); ^{13}C NMR (75 MHz, $CDCl_3$) δ 153.0, 140.2, 136.3, 130.8, 130.5, 129.0, 126.8, 126.1, 125.1, 124.6, 123.8, 122.6, and 120.8 ppm. Anal. Calcd for $C_{13}H_9NS_2$: C, 64.10; H, 3.72. Found: C, 64.14; H, 3.67.

Reaction between *N*-(2-Benzothienyl)iminodiphenylmethylphosphorane and Furan-2-carbaldehyde. A 50.0 mg (0.14

mmol) sample of iminophosphorane **1** and 11.9 μL (0.141 mmol) of furan-2-carbaldehyde in dry toluene (3 mL) were stirred at 100 °C in N_2 atmosphere for 22 h. After solvent removal in vacuo the crude mixture was purified on silica gel with a 8:2 mixture of hexanes and ethyl acetate. Two isomeric imines were recovered: **3a**, 16.0 mg of yellow powder at R_f 0.70 (50% yield), and **6a**, 9.5 mg of yellow powder, R_f 0.60 (30% yield). Compound **6a**: mp 80 °C. ^{1}H NMR (500 MHz, $CDCl_3$) δ 8.32 (s, 1 H), 8.11−8.08 (m, 1 H), 7.60 (s, 1 H), 7.25−7.20 (m, 2 H), 7.16−7.13 (m, 1 H), 6.92−6.91 (m, 1 H), 6.55−6.54 (m, 1 H), and 6.34−6.33 ppm (m, 1 H); MS, *m*/*z*, 227 (M^+). Anal. Calcd for $C_{13}H_9NOS$: C, 68.70; H, 3.99. Found: C, 68.85; H, 3.83.

Reaction between *N*-(2-Benzothienyl)iminodiphenylmethylphosphorane and Thiophene-2-carbaldehyde. A 49.3 mg (0.142 mmol) sample of iminophosphorane **1** and 13.2 μL (0.141 mmol) of thiophene-2-carbaldehyde in dry toluene (3 mL) were stirred at 100 °C in N_2 atmosphere for 24 h. After solvent removal in vacuo the crude mixture was purified on silica gel with a 8:2 mixture of hexanes and ethyl acetate. Two isomeric imines were recovered: **3b**, 26.1 mg of yellow powder at R_f 0.78 (67% yield), and **6b**, 10.7 mg of yellow powder, R_f 0.66 (33% yield). Compound **6b**: mp 112−115 °C. ^{1}H NMR (300 MHz, $CDCl_3$) δ 8.56 (s, 1 H), 8.29 (d, 1 H, J = 5 Hz), 7.69 (d, 1 H, J = 5 Hz), 7.50−7.42 (m, 2 H), 7.22−7.10 (m, 3 H), and 6.90−6.78 ppm (m, 1 H); ^{13}C NMR (75 MHz, $CDCl_3$) δ 150.0, 148.5, 143.0, 140.0, 135.5, 132.5, 131.5, 128.0, 126.0, 125.0, 124.5, 124.0, and 122.50 ppm. Anal. Calcd for $C_{13}H_9NS_2$: C, 64.16; H, 3.73. Found: C, 64.32; H, 3.60.

Reaction between *N*-(2-Benzothienyl)iminodiphenylmethylphosphorane and Furan-3-carbaldehyde. A 50.0 mg (0.14 mmol) sample of iminophosphorane **1** and 11.9 μL (0.141 mmol) of furan-3-carbaldehyde in dry toluene (3 mL) were stirred at 100 °C in N_2 atmosphere for 22 h. After solvent removal in vacuo the crude mixture was purified on silica gel with a 8:2 mixture of hexanes and ethyl acetate. Two isomeric imines were recovered: **5a**, 14.0 mg of yellow powder at R_f 0.86 (44% yield), and **7a**, 9.0 mg of dark yellow oil, R_f 0.78 (28% yield). Compound **7a**: ^{1}H NMR (300 MHz, $CDCl_3$) δ 8.44 (s, 1 H), 8.26 (d, 1 H, J = 3 Hz), 7.86 (s, 1 H), 7.78−7.72 (m, 1 H), 7.58−7.52 (m, 1 H), 7.44 (s, 1 H), 7.28−7.21 (m, 1 H), 7.19−7.13 (m, 1 H), and 6.70 ppm (s, 1 H). Anal. Calcd for $C_{13}H_9NOS$: C, 68.70; H, 3.99. Found: C, 68.85; H, 3.75.

Reaction between *N*-(2-Benzothienyl)iminodiphenylmethylphosphorane and Thiophene-3-carbaldehyde. A 47.6 mg (0.137 mmol) sample of iminophosphorane **1** and 12.0 μL (0.137 mmol) of thiophene-3-carbaldehyde in dry toluene (3 mL) were stirred at 100 °C in N_2 atmosphere for 24 h. After solvent removal in vacuo the crude mixture was purified on silica gel with a 8:2 mixture of hexanes and ethyl acetate. Two isomeric imines were recovered: **5b**, 14.1 mg of yellow powder at R_f 0.78 (42% yield), and **7b**, 7.3 mg of yellow oil, R_f 0.66 (21% yield). Compound **7b**: ^{1}H NMR (300 MHz, $CDCl_3$) δ 8.47 (s, 1 H), 8.13 (d, 1 H, J = 5.7 Hz), 7.75−7.67 (m, 1 H), 7.36−7.32 (m, 1 H), 7.24−7.20 (m, 3 H), and 7.14−7.04 ppm (m, 2 H). ^{13}C NMR (75 MHz, $CDCl_3$) δ 151.0, 149.0, 143.0, 140.0, 135.5, 131.0, 130.5, 129.0, 126.5, 124.5, 121.5, and 121.0 ppm. Anal. Calcd for $C_{13}H_9NS_2$: C, 64.16; H, 3.73. Found: C, 64.02; H, 3.87.

Reaction between *N*-(2-Benzothienyl)iminodiphenylmethylphosphorane and 5-Nitrofuran-2-carbaldehyde. A 56.1 mg (0.161 mmol) sample of iminophosphorane **1** and 23.0 mg (0.161 mmol) of 5-nitrofuran-2-carbaldehyde in dry toluene (3.5 mL) were stirred at 100 °C in N_2 atmosphere for 20 h. After solvent removal in vacuo the crude was purified on silica gel with a 8:2 mixture of hexanes and ethyl acetate. Compound **3c**, 37.3 mg (85% yield), was recovered; mp 70 °C. ^{1}H NMR (300 MHz, $CDCl_3$) δ 8.30 (s, 1 H), 7.80−7.70 (m, 2 H), 7.56 (s, 1 H), 7.43 (d, 1 H, J = 6 Hz), 7.41−7.34 (m, 2 H), and 7.20 ppm (d, 1 H, J = 6 Hz); ^{13}C NMR 153.0, 152.8, 152.1, 144.9, 138.6, 137.0, 126.6, 125.5, 125.1, 124.8, 122.6, 115.0, and 113.0 ppm. Anal. Calcd for $C_{13}H_8N_2O_3S$: C, 57.35; H, 2.96. Found: C, 57.52; H, 2.90.

Reaction between *N*-(2-Benzothienyl)iminodiphenylmethylphosphorane and 5-Nitrothiophene-2-carbaldehyde. A 58.3 mg (0.168 mmol) sample of iminophosphorane **1** and 23.4 mg (0.168 mmol) of 5-nitrothiophene-2-carbaldehyde in dry toluene (3.5 mL) were stirred at 100 °C in N_2 atmosphere for 22 h. After solvent removal in vacuo the crude was purified on silica gel with a 8:2 mixture of hexanes and ethyl acetate. Compound **3d** (39.5 mg, 89% yield) was recovered; mp 70 °C. ^{1}H NMR (300 MHz, $CDCl_3$) δ 8.48 (s, 1 H), 7.93 (d, 1 H, J = 6 Hz), 7.80−7.72 (m, 2 H), 7.50 (s, 1 H), and 7.43−7.34 ppm (m, 3 H); ^{13}C NMR (75 MHz, $CDCl_3$) δ 151.8, 149.2, 148.0, 138.6, 137.0, 129.9, 129.4, 126.4, 125.1, 124.8, 124.6, and 122.8 ppm. Anal. Calcd for $C_{13}H_8N_2O_2S_2$: C, 57.15; H, 2.80. Found: C, 57.30; H, 2.65.

Thieno[2,3-*c*]pyridino[2,3-*d*]benzo[*b*]thiophene (8). Thick oil, 3 mg (30%). ^{1}H NMR (300 MHz, $CDCl_3$) δ 8.83 (s, 1 H), 8.2−8.15 (m, 1 H), 7.9−7.85 (m, 1 H), and 7.6−7.35 ppm (m, 4 H); MS, *m*/*z* 241 (M^+, 100). Anal. Calcd for $C_{13}H_7NS_2$: C, 64.70; H, 2.92. Found: C, 64.67; H, 2.88.

Thieno[3,2-*c*]pyridino[2,3-*d*]benzo[*b*]thiophene (9). Thick oil, 6 mg (61%). ^{1}H NMR (300 MHz, $CDCl_3$) δ 8.96 (s, 1 H), 8.81 (m, 1 H), 8.32−8.25 (m, 1 H), 8.20−8.15 (m, 1 H), 8.00−7.95 (m, 1 H), 7.75−7.70 (m, 1 H), and 7.55−7.51 ppm (m, 1 H); ^{13}C NMR (75 MHz, $CDCl_3$) δ 168.5, 149.8, 141.6, 138.0, 134.4, 131.4, 128.1, 127.1, 125.6, 123.5, 122.2, 121.7, and 120.3 ppm; MS, *m*/*z* 241 (M^+, 100). Anal. Calcd for $C_{13}H_7NS_2$: C, 64.70; H, 2.92. Found: C, 64.64; H, 2.98.

Computational Methods. Molecular geometries were optimized by using the Kohn−Sham density functional theory (DFT)[8] with the 6-31G(d) basis set and the Becke three-parameters hybrid exchange-correlation functional known as B3LYP.[9] Analytical evaluation of the energy second derivative matrix with respect to Cartesian coordinates (Hessian matrix) at the same level of approximation confirmed the nature of minima of transition structures of the energy surface points associated with the optimized structures.

A test of the reliability of the basis set has been performed by increasing the basis set to the 6-311G(2d,p) level of approximation. The refined geometries of the *cis*-1 and *trans*-1 imines from furan-2-carbaldehyde (look below for the structure labeling) are substantially coincident to the 6-31G* geometries. The energy difference between the two structures is 7.4 kcal/mol with both basis sets.

Time dependent density functional theory (TD-DFT)[10,11] allowed the computation of vertical excitation energies, oscillator strengths, and excited-state compositions in terms of monoelectronic excita-

(8) Parr, R. G.; Yang, W. *Density Functional Theory of atoms and molecules*; Oxford University Press: New York; Clarendon Press: Oxford, 1989.

(9) Becke, A. D. *J. Chem. Phys.* **1993**, *98*, 5648−5652.

(10) Casida, M. E. In *Recent Advances in Density Functional Methods*; Chong, D. P., Ed.; World Scientific: Singapore, 1995; Vol. 1, pp 155−192.

(11) Casida, M. E.; Jamorski, C.; Casida, K. C.; Salahub, D. R. *J. Chem. Phys.* **1998**, *108*, 4439−4449.

(12) Becke, A. D. *Phys. Rev. A* **1988**, *38*, 3098−3100.

(13) Lee, C.; Yang, W.; Parr, R. G. *Phys. Rev. B* **1988**, *37*, 785−789.

(14) Frisch, M. J.; Trucks, G. W.; Schlegel, H. B.; Scuseria, G. E.; Robb, M. A.; Cheeseman, J. R.; Zakrzewski, V. G.; Montgomery, J. A., Jr.; Stratmann, R. E.; Burant, J. C.; Dapprich, S.; Millam, J. M.; Daniels, A. D.; Kudin, K. N.; Strain, M. C.; Farkas, O.; Tomasi, J.; Barone, V.; Cossi, M.; Cammi, R.; Mennucci, B.; Pomelli, C.; Adamo, C.; Clifford, S.; Ochterski, J.; Petersson, G. A.; Ayala, P. Y.; Cui, Q.; Morokuma, K.; Malick, D. K.; Rabuck, A. D.; Raghavachari, K.; Foresman, J. B.; Cioslowski, J.; Ortiz, J. V.; Stefanov, B. B.; Liu, G.; Liashenko, A.; Piskorz, P.; Komaromi, I.; Gomperts, R.; Martin, R. L.; Fox, D. J.; Keith, T.; Al-Laham, M. A.; Peng, C. Y.; Nanayakkara, A.; Gonzalez, C.; Challacombe, M.; Gill, P. M. W.; Johnson, B. G.; Chen, W.; Wong, M. W.; Andres, J. L.; Head-Gordon, M.; Replogle, E. S.; Pople, J. A. *Gaussian 98*, revision A.11; Gaussian, Inc.: Pittsburgh, PA, 2001.

(15) Schaftenaar, G.; Noordik, J. H. *J. Comput.-Aided Mol. Des.* **2000**, *14*, 123−134 (http://www.cmbi.ru.nl/molden/molden.html).

tions between occupied and virtual orbitals. These computations were performed at the B3LYP/6-31G(d) level of approximation on the B3LYP/6-31G(d) geometries.

In some circumstances, as evidenced in the text, geometry optimizations have been performed at the Hartree−Fock level and 6-31G(d) basis set. Such computations have been followed by excited states computations by means of configuration interaction based on single excitations (CIS) with the 6-31G(d) basis set. Similarly, DFT and TD-DFT computations based on the pure exchange-correlation functional BLYP (Becke's 1988 exchange functional[12] and correlation functional of Lee,Yang, and Parr[13]) have been performed on some compounds.

All the calculations were performed with the Gaussian98 program.[14] Figures 2, 5, an 11 have been produced by using the Molden program.[15]

Acknowledgment. MIUR is gratefully acknowledged for financial support to this research.

Supporting Information Available: ^{1}H and ^{13}C NMR spectra of compounds **1**, **3a**−**d**, **5a**,**b**, **6a**,**b**, **7a**,**b**, **8**, and **9**; Cartesian coordinates, a complete list of frequencies, and a list of total energies for all the minimized structures. This material is available free of charge via the Internet at http://pubs.acs.org.

JO0605501